The Astrophysical Journal, 669:585–599, 2007 November 1

MAGNETICALLY DRIVEN EXPLOSIONS OF RAPIDLY ROTATING WHITE DWARFS FOLLOWING ACCRETION-INDUCED COLLAPSE

L. Dessart,[1] A. Burrows,[1] E. Livne,[2] and C. D. Ott[1]

Received 2007 May 24; accepted 2007 July 17

ABSTRACT

We present two-dimensional multigroup flux-limited diffusion magnetohydrodynamics (MHD) simulations of the accretion-induced collapse (AIC) of a rapidly rotating white dwarf. We focus on determining the dynamical role of MHD processes after the formation of a millisecond-period proto–neutron star. We find that magnetic stresses lead to a powerful explosion with an energy of a few Bethe, rather than a weak one of at most 0.1 B, with an ejecta mass of $\sim$0.1 $M_\odot$, instead of a few 0.001 $M_\odot$. The core is spun down by $\sim$30% within 500 ms after bounce, and the rotational energy extracted is channeled into magnetic energy that generates a strong magnetically driven wind, rather than a weak neutrino-driven wind. Baryon loading of the ejecta, while this wind prevails, precludes it from becoming relativistic. This suggests that a γ-ray burst (GRB) is not expected to emerge from such AICs during the early proto–neutron star phase, except in the unlikely event that the massive white dwarf in this AIC context has sufficient mass to lead to black hole formation. In addition, we predict both negligible ^{56}Ni production (that should result in an optically dark, adiabatically cooled explosion), and the ejection of 0.1 $M_\odot$ of material with an electron fraction of 0.1–0.2. Such pollution by neutron-rich nuclei puts strong constraints on the possible rate of such AICs. Moreover, being free from ''fallback,'' such highly magnetized millisecond-period proto–neutron stars may, as they cool and contract, become magnetars, and the magnetically driven winds may later transition into Poynting-flux-dominated and relativistic winds, eventually detectable as GRBs at cosmological distances. The likely low event rate of AICs, however, will constrain them to be, at best, a small subset of GRB and/or magnetar progenitors.

Subject headings: gamma rays: bursts — neutrinos — stars: neutron — stars: rotation — supernovae: general — white dwarfs

Online material: color figures

1. INTRODUCTION

Some white dwarfs, located in binary systems, are thought to lead to thermonuclear runaways and Type Ia supernovae, a circumstance in which a Chandrasekhar mass carbon and oxygen core is incinerated, on a timescale of $\sim$1 s, to intermediate-mass and iron-peak elements. In the single-degenerate scenario, the white dwarf accretes material from a hydrogen or helium donor star. Aided by the stabilizing effect of fast and differential rotation (Yoon et al. 2004), it reaches the $\sim$1.4 $M_\odot$ Chandrasekhar limit and explosively burns carbon and oxygen under degenerate conditions. However, for sufficiently high mass accretion rates, carbon and oxygen may burn under nondegenerate conditions to allow the formation of a high-density ONeMg core which, on achieving the Chandrasekhar mass, collapses on a dynamical timescale of $\sim$100 ms (Nomoto & Kondo 1991; Nomoto et al. 1995; Gutierrez et al. 1996; Gil-Pons & García-Berro 2001). In the double-degenerate scenario, two white dwarfs in a short-period binary system eventually coalesce to form a massive white dwarf that exceeds the Y_e-corrected Chandrasekhar mass limit. smooth-particle hydrodynamics (SPH) simulations (Benz et al. 1990; Mochkovitch & Livio 1989, 1990; Segretain et al. 1997; Guerrero et al. 2004; Yoon et al. 2007) predict the formation of a complex object composed of a cold, slowly rotating core, surrounded by a hot and fast-rotating envelope, and, farther out, by some residual mass in a Keplerian disk. Depending on the temperature in the envelope, the mass accretion rate on the newly formed white dwarf, and the mass of each white dwarf component, either a Type Ia or accretion-induced collapse (AIC) are possible. Overall, the occurrence rate of the AIC of white dwarfs is difficult to determine reliably, although it seems unlikely that they occur more frequently than once per 20–50 Type Ia event (Yungelson & Livio 1998, 2000; Madau et al. 1998; Fryer et al. 1999; Nelemans et al. 2001a, 2001b; Blanc et al. 2004; Mannucci et al. 2005; Belczynski et al. 2005; Greggio 2005; Scannapieco & Bildsten 2005; Dessart et al. 2006b, hereafter D06).

In this work, we focus on the subset of accreting white dwarfs that form ONeMg cores, which, due to their high central density and mass, collapse to form a neutron star. The formation path followed, either through accretion from, or coalescence with, a companion, suggests a large angular momentum budget for the resulting white dwarf. Such white dwarfs rotate differentially, with a specific angular momentum that increases outward, and can be dynamically stable well above the canonical Chandrasekhar mass of $\sim$1.4 $M_\odot$, reaching theoretical masses as high as 4.1 $M_\odot$ (Ostriker & Bodenheimer 1968; Hachisu 1986; Yoon & Langer 2005). The precise distribution of the angular momentum inside the star is not accurately known, in particular since magnetic torques may spin down the core and enforce solid-body rotation, producing an even more slowly rotating core than currently predicted by SPH simulations ($\sim$20 s period). In any case, the overlying envelope is fast-rotating, and the resulting

[1] Department of Astronomy and Steward Observatory, The University of Arizona, Tucson, AZ 85721; luc@as.arizona.edu, burrows@as.arizona.edu, cott@as.arizona.edu.

[2] Racah Institute of Physics, The Hebrew University, Jerusalem, Israel; eli@frodo.fiz.huji.ac.il.

progenitor is strongly aspherical (Guerrero et al. 2004; Yoon et al. 2007).[3]

The collapse of ONeMg cores has been investigated in the past both in the context of white dwarfs (Baron et al. 1987b; Woosley & Baron 1992; Fryer et al. 1999; D06) and in the context of 8–10 $M_\odot$ stars (i.e., low-mass massive stars; Hillebrandt et al. 1984; Mayle & Wilson 1988; Baron et al. 1987a; Kitaura et al. 2006; Burrows et al. 2007b). In D06, we presented results of radiation hydrodynamics simulations of the AIC of white dwarfs that extended these past investigations simultaneously to include multidimensionality, multigroup flux-limited diffusion for multiflavor neutrino transport, and, perhaps most importantly, rapid rotation. We focused on the 1.46 and the 1.92 $M_\odot$ models of Yoon & Langer (2005) and found for the latter that fast rotation led to numerous striking features, e.g., aspherical collapse, aspherical bounce, polar-confined explosions, polar-enhanced neutrino radiation fields, gravity-darkened neutron stars, oblateness of the neutron stars formed, and a residual Keplerian disk. In this scenario, the differential rotation that results from core collapse sets the stage whereby, from initial seeds in the poloidal component, a magnetic field may exponentially grow on a timescale of a rotation period by magnetorotational instability (MRI; Balbus & Hawley 1991; Pessah & Psaltis 2005; Pessah et al. 2006a, 2006b; Etienne et al. 2006), acting on the poloidal and toroidal fields. If equipartition between the magnetic energy and the differential rotational energy is reached at saturation, very substantial fields may be generated for the fastest rotators (Shibata et al. 2006). The 1.92 $M_\odot$ AIC white dwarf studied in D06, with an initial $T/|W|$ of 10% (W is the gravitational energy of the initial equilibrium configuration, and T is the initial rotational kinetic energy), represents a good candidate for MHD effects after core bounce. Unfortunately, it is not feasible, even with modern supercomputers, both to follow the multidimensional evolution of a multigroup neutrino field for three species and to resolve finely enough the scales over which the magnetorotational instability operates. To circumvent this difficulty, we start with fields that are strong enough to reach soon after core bounce (after a few tens of rotation periods) the saturation values they would have reached had the MRI operated. Magnetic-field amplification then results exclusively from compression and winding. This is the approach followed in Burrows et al. (2007a), where we presented results for magnetically driven supernova explosions of massive star progenitors in the context of fast rotation.

The central motive for this work is to go beyond the investigations of D06 and to study the potential role of MHD effects, adopting initial fields that will be commensurate at saturation with values expected from equipartition with the free energy of rotation in the differentially rotating surface layers of the rotating collapsed core. Thus, we investigate the MHD effects that may arise during the collapse phase and the few hundreds of milliseconds that directly follow the formation of the neutron star. Guided by our simulations, we comment on past and current suggestions that the AIC of white dwarfs are potential gamma-ray burst (GRB) and/or magnetar progenitors, or are important production sites of r-process nuclei.

In the next section, we discuss (briefly) the VULCAN/2D code, and the numerical setup, as well as the 1.92 $M_\odot$ AIC model we focus on. The details of the code can be found in Livne et al. (2004, 2007), Dessart et al. (2006a), and Burrows et al. (2007c), and the AIC initial model properties are given in D06. In § 3, we describe the results of our simulations, and compare a reference model with weak initial fields to another model with strong initial fields. We discuss our results in the broader astrophysical context in § 4. In § 4.1, we summarize the main MHD effects we identify, and in § 4.2 we discuss the potential nucleosynthetic yields. In § 4.3, we discuss potential electromagnetic displays from AICs, and whether they can be γ-ray bursts, and in § 4.4 we discuss the ultimate fate of these rare objects. Finally, in § 5, we present our conclusions.

2. MODEL AND PROGENITOR PROPERTIES

The models presented in this work derive from the 1.92 $M_\odot$ model of D06 (see their § 2), originally produced in Yoon & Langer (2005). The initial density, temperature, composition, and angular velocity distributions are coincident with those used in D06. To summarize, the central density is $\rho_c = 5 \times 10^{10}$ g cm^{-3}, the temperature is given by $T(r,z) = T_c(\rho_c/\rho(r,z))^{0.35}$, with $T_c = 1.3 \times 10^{10}$ K (r and z are the standard cylindrical coordinates), the initial electron fraction (Y_e) is 0.5 throughout the grid, and the central angular velocity is 20.4 rad s^{-1} (with a period of 0.3 s). To minimize the dynamical influence of the medium surrounding the white dwarf, which needs to be initially defined in our Eulerian approach, we assign it properties that correspond to the low-density, low-temperature edge of our equation of state (EOS; see also below), i.e., a density of 10^3 g cm^{-3}, and a temperature of 4×10^8 K. Furthermore, we also assign it a negligible angular velocity. Initially, the polar (equatorial) radius is 660 km (2350 km), the total angular momentum is 0.1092 B s (1 B $\equiv 10^{51}$ erg), the total rotational energy T is 1.057 B, and the gravitational energy $|W|$ is 12.69 B. This model thus starts with a ratio $T/|W|$ of 0.083, indicative of the large angular momentum budget in the progenitor white dwarf. We refer the reader to § 2 and Figure 1 of D06 for a detailed description of this initial model, with two-dimensional (2D) representations of the original distribution of the density, temperature, and angular velocity.

The magnetic field morphology we adopt is uniform inside a sphere of radius 600 km (the poloidal component has a z-orientation, i.e., is aligned with the axis of rotation), and dipolar beyond. Note that the original model of Yoon & Langer (2005) corresponds to an equilibrium configuration that results from the balance between gravitational, rotational, and thermal energy, and conveys no information on the magnetic-field morphology and magnitude. One may argue that magnetic torques would enforce solid-body rotation in the initial model we adopt from Yoon & Langer (2005), making our approach inadequate. We propose in this work that even such super-Chandrasekhar white dwarfs are unlikely to lead to black hole formation, so the differential rotation of our initial model does not compromise our conclusions in this respect. Our main assumption is that such torques may alter the rotational profile, but not significantly reduce the overall rotational energy budget of the white dwarf, preserving its status as a fast rotator. Furthermore, the initial differential nature of the rotation is not essential, since gravitational collapse will naturally lead to it. For the binary merger scenario, magnetic torques would likely not have sufficient time to sizably

[3] Observationally inferred rotation rates of white dwarfs are, however, generally modest, a fact attributed to the copious angular momentum losses during their evolution, even for isolated white dwarfs (Koester et al. 1998; Berger et al. 2005; Valyavin et al. 2005; Karl et al. 2005). Magnetic, fast-rotating white dwarfs in binary systems may also undergo considerable spin-down, caused by magnetic torquing of the envelope (Ikhsanov 1999). Merger events show, by contrast, a potential for the production of fast-rotating white dwarfs, with properties more germane to the present discussion (Ferrario & Wickramasinghe 2005). If fast rotation of either the core or the envelope were compromised, the outcome of the AIC would be more suitably described by the simulation of D06 for the 1.46 $M_\odot$ model, rather than the 1.92 $M_\odot$ model described here or in D06.

torque the white dwarf before core collapse. Little is known about the core magnetic fields of white dwarfs, and even less about that fraction of them that may lead to AIC and fast rotation, nor do we know how the poloidal and toroidal components relate. Again, the key here is that we assume that starting from a given initial seed poloidal field, the magnetorotational instability will result in the exponential growth of the magnetic energy after bounce, and then saturate, after a few tens of rotation periods, at the field we obtain here. By that time, we expect that the system will have lost memory of the magnetic field distribution it started with.

In practice, we perform simulations with an initial poloidal field of 10^{11} G for model B11 and of 10^{12} G for model B12, while in both cases we use a toroidal field of 10^8 G (these values are at the white dwarf center). Note that the magnetic field amplification at bounce resulting from compression alone will lead to an enhancement of the magnetic field by a factor of only $(\rho_{\rm nuclear}/\rho_c)^{2/3} \sim 300$, because of the very high initial central density ($\rho_c = 5 \times 10^{10}$ g cm^{-3}). For a star with an initial central density of 5×10^9 g cm^{-3}, a typical value at the onset of core collapse for a massive-star progenitor, the field amplification would be by a factor of $\sim$1200 instead, so that an initial field of 2×10^{11} G would achieve a comparable magnetic field at bounce. Hence, initial field values must always be interpreted together with the initial central densities to properly gauge the amplification generated by compression. The choice of a predominantly poloidal component is essential in our approach, allowing for the growth of the toroidal component after the initial compression phase. If the MRI operated, the exponential growth of both components of the magnetic field, permitted by the large budget of free energy of rotation, would reach saturation values that are orders of magnitude above the initial seed values. Hence, in this context, the main limiting factor is the rotational energy budget rather than the initial properties of the field.

The evolution of the B11 model is similar to that of the nonmagnetic 1.92 $M_\odot$ AIC model presented in D06, and we use it to gauge the importance of MHD effects in the B12 model. The lack of magnetic effects in the B11 model is a clear sign that we do not resolve the MRI, since otherwise we would observe magnetic fields that saturate at values similar to those seen in the B12 model, and we do not. Note that the 1.92 $M_\odot$ progenitor model we discuss in this work is not meant to be representative of AICs in nature, as, indeed, these may come with a range of angular momenta or masses. Our B12 model is chosen because it is one example where all conditions are prime for the generation of MHD effects, thus occupying one extreme when compared to, for example, the more slowly rotating and quasi-spherical 1.46 $M_\odot$ model simulated in D06. This approach allows us, we hope, to bracket the range of outcomes for AICs.

We adopt the same spatial grid as D06, with a Cartesian mapping of the region inside a spherical radius of 20 km and a spherical-polar grid out to a maximum radius of 4000 km. The maximum resolution of 0.48 km is reached in the Cartesian inner region, and the minimum resolution is 100 km at the maximum radius, with 71 regularly spaced angular zones covering 90°. In D06, we found that the top/bottom symmetry was perfectly preserved in the 180° simulations of the 1.46 $M_\odot$ AIC model. We speculate that the postbounce time to explosion is so short that convection and the standing accretion shock instability (SASI; Blondin et al. 2003; Foglizzo et al. 2006) cannot grow to any sizable level, perhaps inhibited by the strong differential rotation (Burrows et al. 2007a). Hence, we save time and opt for higher resolution by restricting our investigation to one hemisphere.

The simulations we present here constitute the state of the art, combining in the dynamical equations the effects of both magnetic field and neutrino transport. As in D06, we employ the approximation of multigroup flux-limited diffusion, using 16 logarithmically spaced energy groups between 2.5 and 220 MeV, for three neutrino species (electron neutrino ν_e, antielectron neutrino $\bar{\nu}_e$, and a third entity grouping the remaining neutrinos, designated "ν_μ"). We also employ a tabulated version of the Shen (1998) EOS (see Dessart et al. 2006a for details). Finally, the gravitational potential is computed using a multipole solver, with a decomposition in spherical harmonics that extends to $l = 32$. Again, the VULCAN/2D code and our standard approach to modeling core collapse are described in Livne et al. (2004, 2007), Dessart et al. (2006a), and Burrows et al. (2007c), while further details on the AIC of white dwarfs have been given in D06.

3. DESCRIPTION OF THE EXPLOSION

In this section, we present the collapse, bounce, and explosion phases of the 1.92 $M_\odot$ AIC white dwarf model computed by, and with the method of, Yoon & Langer (2005). In contrast to a similar investigation performed and analyzed in great detail in D06, magnetic fields are now included, leading to little qualitative, but considerable quantitative, changes in the results. For completeness, we briefly review the important phases of the explosion arising from such AIC of white dwarfs. Important results are discussed again, and in a broader context, in § 4.

Due to the high central density of such white dwarfs (above $\sim 10^{10}$ g cm^{-3}, and here set to 5×10^{10} g cm^{-3}), electron captures on nuclei lead to the collapse of the ONeMg core on a near dynamical timescale. About 37 ms after the start of the simulation, the inner core reaches nuclear densities, i.e., $\gtrsim 2 \times 10^{14}$ g cm^{-3}. A shock wave is born that propagates outward, but weakens due to the huge energy losses associated with the burst of electron neutrinos and the photodissociation of nuclei in the infalling outer-core material. Along the equator, where the accreting material enjoys sizable centrifugal support, the shock first propagates quickly due to the reduced accretion rate, but eventually stalls due to its sustained magnitude. By contrast, along the polar direction, where the density profile is much steeper, after at first stalling due to the higher accretion rate, the shock soon encounters the layers that were formerly at the surface of the white dwarf. As no further accretion occurs, the shock blasts out of the white dwarf along the pole only 80–100 ms after bounce, and an explosion is initiated. Up to that point, the simulations B11 and B12 show the same qualitative and quantitative properties, suggesting that magnetic effects on the dynamics are weak or negligible during the first $\sim$100 ms postbounce evolutionary phases of the AIC.

However, it takes $\sim$100 ms in the B12 model to amplify the magnetic field to a value such that magnetic pressure and gas pressure are comparable, at first in the polar regions at a few tens of kilometers from the proto–neutron star (PNS) center. Compression from the progenitor to a high-density collapsed configuration is the early cause of magnetic field amplification, but later it arises from the winding of the poloidal field and the continued accretion of the magnetized envelope, spinning up as it collapses (see discussion in Burrows et al. 2007a). The toroidal field eventually dominates over the poloidal field component in the inner few hundred kilometers by, typically, 1–2 orders of magnitude. We speculate that the magnetic properties at $\sim$100 ms after bounce are comparable to what would be obtained with a fully resolved MRI. Note that in our simulations, no significant convection develops behind the shock, as required

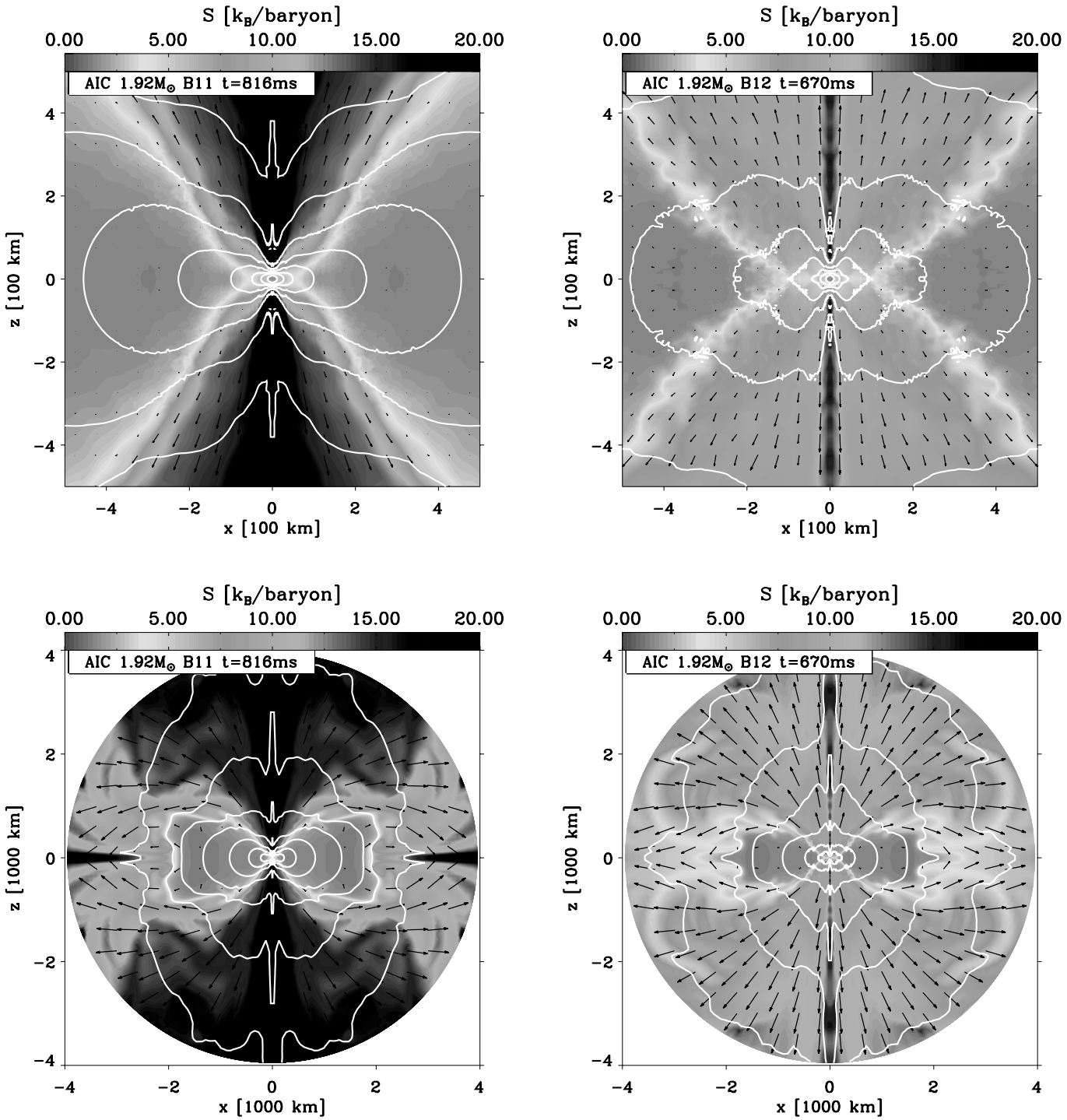

FIG. 1.—*Top*: Color map of the entropy for the B11 (*left*) and B12 (*right*) models, at 816 and 670 ms after bounce, respectively, and in the inner 1000×1000 km^2, using black vectors to represent the velocity field (the length is saturated at 5000 km s^{-1}, corresponding to 5% of the width of the display). We also overplot isodensity contours, shown for every decade starting at 10^{14} g cm^{-3}. *Bottom*: Same as for the top panels, but extending the maximum displayed radius to 4000 km, the maximum grid radius in our simulations. The saturation length for the velocity vectors is now 10000 km s^{-1}. (See text for discussion.) [*See the electronic edition of the Journal for a color version of this figure*.]

for the α^2 and α-Ω dynamo invoked for magnetic field amplification by Duncan & Thompson (1992) and Thompson & Duncan (1995). In any case, in the B12 model after $\sim$100 ms, the resulting large magnetic pressure and associated gradient at the surface of the neutron star power a strong magnetically driven outflow that expands in the previously excavated polar regions of the progenitor white dwarf. There is here an analogy with magnetic tower formation in magnetic, differentially rotating disks (Lynden-Bell 1996, 2003; Uzdensky & MacFadyen 2006), since the general picture is of magnetic field amplification in a medium that exerts pressure anisotropically. Here, the presence of and excavated polar regions and a dense centrifugally supported fat disk at lower latitudes offers a natural confinement mechanism for the magnetically driven explosion. Hoop stresses act poorly to confine the blast, since wind particle trajectories originate at the neutron star surface over all latitudes

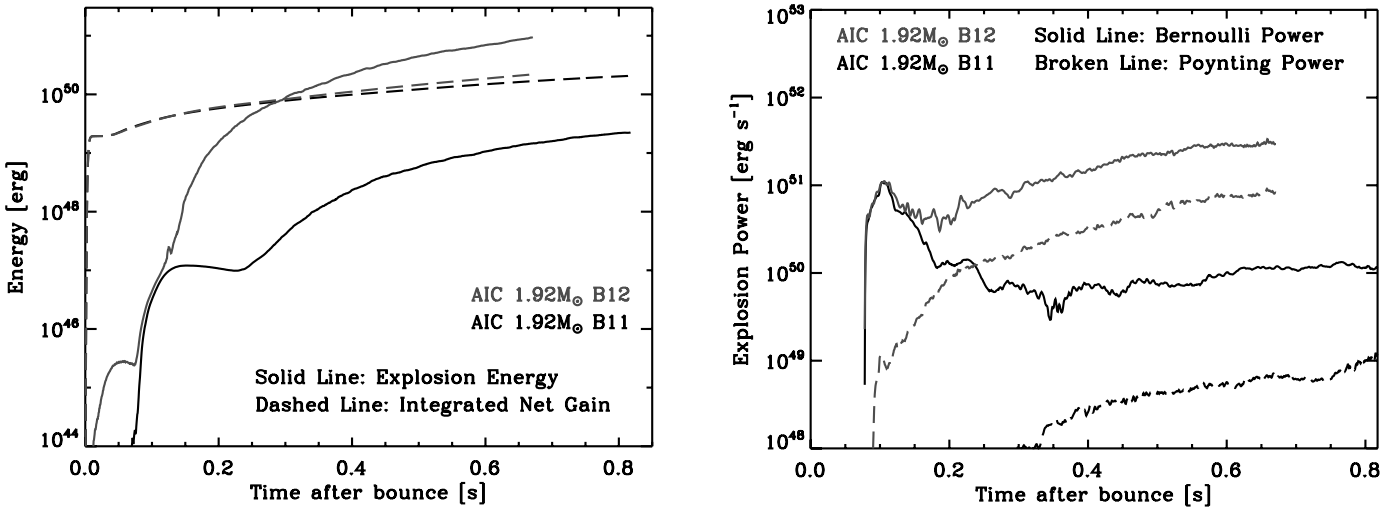

FIG. 2.—*Left*: Time evolution for the 1.92 $M_\odot$ model of Yoon & Langer (2005), with either low (*black*) or high (*red*) initial magnetic fields, of the total energy associated with the ejecta (*solid line*; accounting for gravitational, radial and rotational kinetic, thermal, and magnetic energy components) and the total integrated net neutrino energy gain (*dashed line*). *Right*: Same as left, but for the Bernoulli (*solid line*) and Poynting (*dashed line*) powers in the ejecta, computed by integrating the corresponding flux over a radial shell at 500 km. [*See the electronic edition of the Journal for a color version of this figure.*]

between $\sim 40^\circ$ and 90°.[4] By comparison, in the B11 model, there is a "quiescent" stage after the original blast, with some fallback of a fraction of the ejecta. The explosion is revived after $\sim$300 ms by the birth of a neutrino-driven wind, as discussed in detail in D06. This wind, and the neutrino energy deposition that drives it, are the source of the energy of the explosion in the context of low or negligible magnetic fields. At high B fields, the neutrinos play only a secondary, subdominant, role, and then only after a few hundred milliseconds after bounce.

We have carried out the B11 and B12 simulations up to 816 ms and 670 ms, respectively, after bounce. This constitutes only the very early evolution of the cooling PNS, which typically takes tens of seconds in total when in isolation (Burrows & Lattimer 1986). We show the entropy (color maps) and density (contour lines) distributions in Figure 1 for the B11 (*left*) and B12 (*right*) models at the end of each simulation, encompassing the full grid (*bottom*) or the inner region (*top*). We can identify three different regions: an inner region where an oblate neutron star resides, a prolate mass distribution in the ejecta that is mostly confined to polar or high-latitude regions (above $\sim 40^\circ$), and a fat and Keplerian disk that closely resembles the original lobes of the progenitor white dwarf. We now review in detail each component, together with the global energetics of each explosion.

In the left panel of Figure 2, we show the time evolution, for both models (B12 in red, B11 in black), of the explosion energy (*solid lines*) and integrated net neutrino energy gain as a function of time after bounce (we limit this integration to regions with a mass density less than 10^{10} g cm^{-3}; *dashed lines*). With high initial B field, the explosion energy reaches $\sim$1 B, 2 orders of magnitude higher than in the corresponding low B field case (which explodes underenergetically, but easily, nonetheless), and 1 order of magnitude larger than the integrated net gain through neutrino energy deposition. At low B field, the neutrinos play a critical role in powering the explosion, but the explosion is symptomatically weak, on the order of 0.01 B. In the right panel of Figure 2, we show the power injected into the ejecta, associated both with the Bernoulli[5] flux (*solid line*) and the Poynting flux (*dashed line*) integrated through a sphere at 500 km. Although the Poynting flux decreases roughly as the inverse square of the radius above the neutron star surface, it is larger in the B12 simulation than the Bernoulli flux in the B11 simulation. Combined with the strong Bernoulli flux, the explosion power reaches $\sim$2 B s^{-1}.

This gain in explosion energy stems partly from the extraction of the free energy of rotation of the PNS, the difference between the kinetic energy of rotation and the corresponding energy for solid-body rotation at the same total PNS angular momentum. Selecting the regions inside of a density cut of 10^8, 10^{10}, or 10^{12} g cm^{-3}, the total rotational energy difference between the B11 and the B12 cases is on the order of $\sim$10 B. While a large fraction of this energy is used to expand the PNS, and therefore do work against gravity (where it is the most costly, i.e., at the base of the potential well), some of this energy is made available to the explosion and the growth of the magnetic field, whose associated gradient at the PNS surface is responsible for driving mass outward at the escape speed (Shibata et al. 2006; Burrows et al. 2007a). In the B12 simulation, the PNS density structure is significantly modified, with isodensity contours more spatially separated, and with less contrast between the polar and equatorial radii (see the top row of Fig. 1 for an illustration). Magnetic support is partly responsible for the more extended PNS configuration. As a result, the PNS in the B12 model suffers significant spin-down, another indication that rotational energy has been extracted from the compact object by magnetic torques. The average period in the inner 10^{10} g cm^{-3} increases from 15 to 21 ms, and in the inner 10^{12} g cm^{-3} increases from 2 to 2.5 ms, for models B11 and B12, respectively.

In Figure 3, we illustrate the magnetic properties at the last computed time in each model, for both large and small scales,

[4] The analogy to an infinitely long thin disk threaded by a magnetic field is not strictly applicable.

[5] The Bernoulli flux is defined by the quantity $\rho V_R \times (e_{\rm th} + e_{\rm kin} + e_{\rm rot} + P/\rho - GM_{\rm PNS}/R)$, where V_R is the radial velocity, $e_{\rm th}$ is the thermal energy, $e_{\rm kin}$ and $e_{\rm rot}$ are the (r, z) and rotational kinetic energies, G the gravitational constant, $M_{\rm PNS}$ the PNS mass (taken as the cumulative mass of material with a density greater than 10^{10} g cm^{-3}), and R is the spherical radius. Both the Bernoulli flux and the Poynting flux are then integrated through a sphere at 500 km to give a power, or a luminosity (Fig. 2).

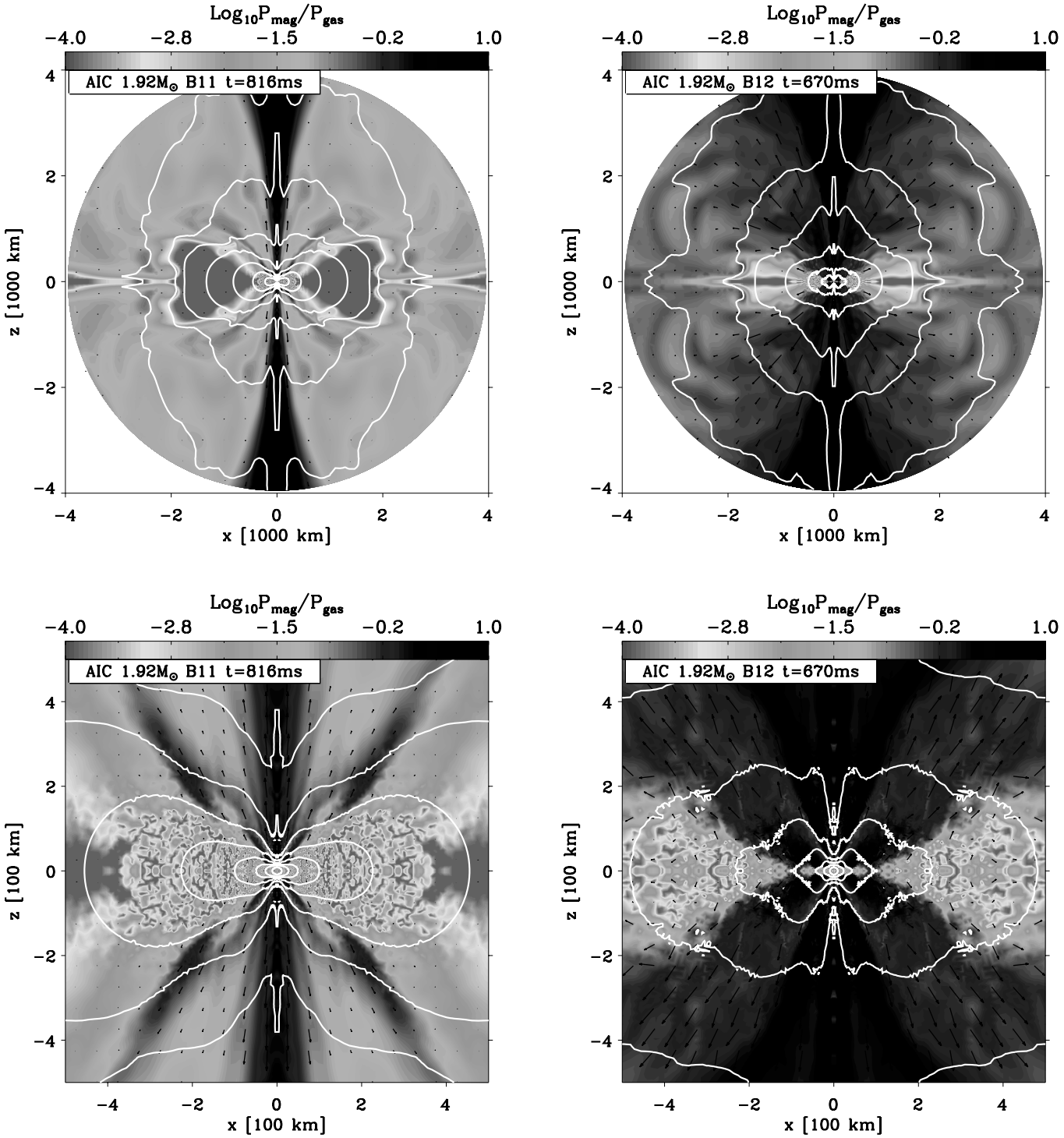

FIG. 3.—*Top*: Color map of the logarithm of the ratio of magnetic pressure to gas pressure for the B11 model (*left*) at 816 ms after bounce, and for the B12 model (*right*) at 670 ms after bounce, using black vectors to represent the Poynting luminosity (the Poynting flux is multiplied by a factor $4\pi R^2$ and the resulting length is saturated at 0.1 B s^{-1}, which corresponds to 5% of the width of the display). We also overplot isodensity contours, for every decade starting at 10^{10} g cm^{-3}, which nicely show their change in morphology from oblate in the neutron star vicinity to prolate at a few thousand kilometers. *Bottom*: Same as top, but now zooming in on the inner few hundred kilometers. The isodensity contours are now plotted up to 10^{14} g cm^{-3}. (See text for discussion.) [*See the electronic edition of the Journal for a color version of this figure*.]

by showing color maps of the ratio of the magnetic pressure to the gas pressure. These are overplotted with vectors depicting the Poynting luminosity (flux scaled by the quantity $4\pi R^2$, where R is the spherical radius). Note how in the B12 model the magnetic pressure is large and comparable to the gas pressure in most of the ejecta. The ejecta retain a higher Poynting flux along the polar direction, even at large distances of a few thousand kilometers, and this is likely caused by the significant confinement of the inner jet. At midlatitudes, the Poynting flux drops faster than the inverse square of the radius. The only excluded regions, where the magnetic field has no substantial effect, are the neutron star core (layers with a local density greater than 10^{12} g cm^{-3})

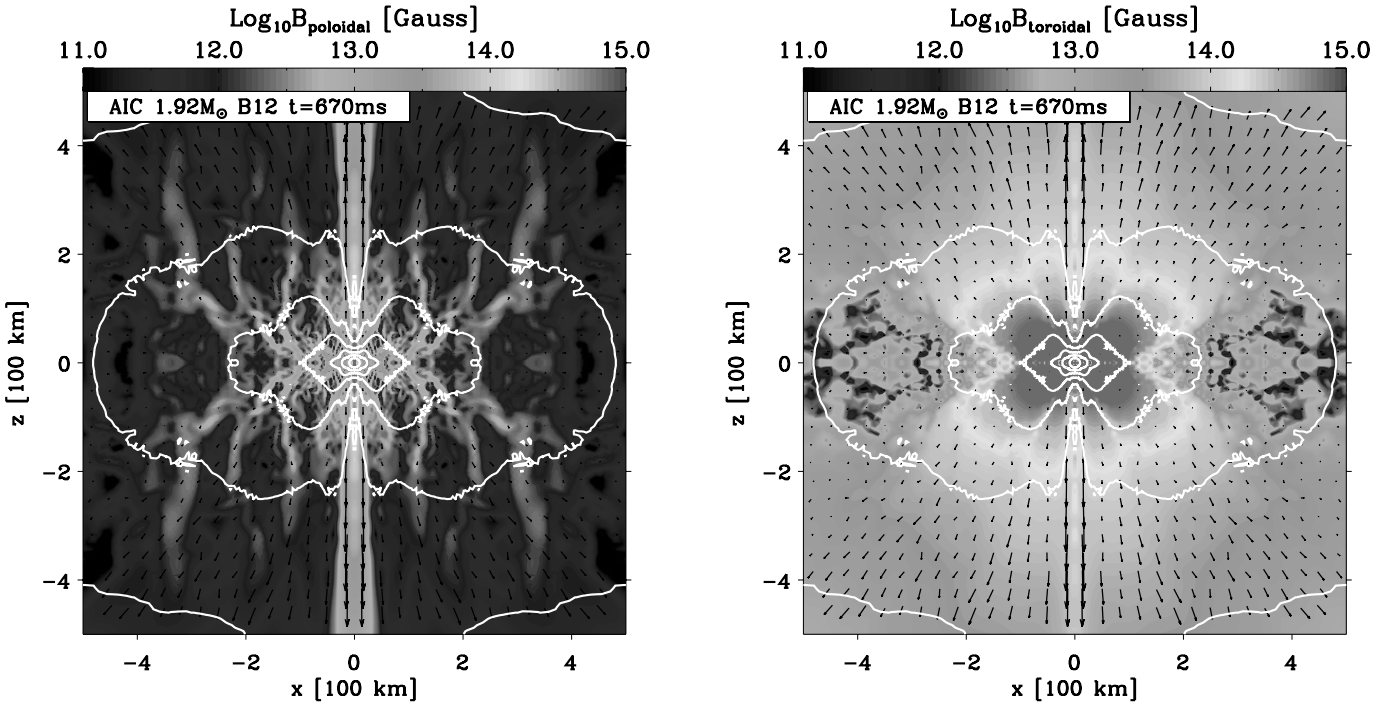

FIG. 4.—*Left*: Color map of the logarithm of the poloidal field magnitude for the B12 model at 670 ms after bounce, using black vectors to represent the velocity (their length is saturated to 7% of the width of the display for a magnitude of 10,000 km s^{-1}). We also overplot isodensity contours, for every decade starting at 10^{14} g cm^{-3} *Right*: Same as left, but for the logarithm of the toroidal field magnitude. (See text for discussion.) [*See the electronic edition of the Journal for a color version of this figure*.]

and the lobes of the progenitor white dwarf (low-density, non-collapsed regions of the progenitor white dwarf). In these latter regions, characterized by large vorticity but little bulk radial advection, we notice large fluctuations in the magnetic to gas pressure ratio, stemming mostly from fluctuations in the magnetic field energy. Although we cannot identify strong convection, stabilized by the differential rotation, moderate velocity shear can induce such local enhancements of the magnetic field.

In Figure 4, we present the spatial distribution in the inner 500 km of each of the poloidal (*left*) and toroidal (*right*) components of the magnetic field for the B12 model at 670 ms after bounce. Unable to resolve the MRI, we predict the dominance of the toroidal component of the magnetic field over the poloidal component, typically by about 2 orders of magnitude, with the exception of the axis region, where it is the strong radial advection of material that generates a strong poloidal field from the original strong toroidal field of the corresponding mass parcel (in the B11 model, equipartition is reached in this region, but the gas density and pressure are 2 orders of magnitude lower than in the same region in the B12 model). While the relative poloidal and toroidal field magnitudes produced by an operating MRI would likely differ, the total magnetic energy we obtain may agree approximately, as it is fundamentally extracted from the (given) free energy of rotation available in the differentially rotating surface layers of the PNS. As in Figure 3, we show in Figure 5 the ratio of the magnetic pressure to the gas pressure, but at 10, 50, 100, and 670 ms after bounce. This figure portrays how the pressure is more and more magnetically dominated directly outside the neutron star; the magnetically driven wind advects highly magnetized material to large distances.

Mass loss in the explosion is considerably enhanced in the B12 model, the cumulative mass expelled being 2 orders of magnitude larger than in the B11 model, i.e., 0.1 $M_\odot$ compared with a few $\times 0.001$ $M_\odot$ (Fig. 6). In both cases, accretion in the equatorial regions, where material is centrifugally supported, is of the order of 0.01 $M_\odot$ s^{-1}. In the low B field case, this is nearly compensated by the mass lost through the neutrino-driven wind. In the B12 model, the mass-loss rate through the magnetically driven wind is nearly 2 orders of magnitude larger, at 0.7 $M_\odot$ s^{-1}, and the nascent neutron star actually loses mass. Interior to a density cut of 10^{10} g cm^{-3}, the PNS baryonic mass is 1.32 $M_\odot$ for the B12 model, compared with 1.47 $M_\odot$ for the B11 model (both at $\sim$500 ms after bounce). At the end of the B12 simulation and at the maximum radius of 4000 km, the ejecta density is 10^5–10^6 g cm^{-3}, and its velocity is 40,000 km s^{-1}. This is about 2 orders of magnitude denser and 20% slower than the neutrino-driven wind we obtain at comparable times in the B11 model. Hence, while the ejecta are magnetically driven, they are not Poynting flux dominated and they are even more nonrelativistic.

In D06, we found that the electron fraction of the ejected material was bimodal, with symmetric material of high entropy (i.e., $\sim$25 k_B baryon^{-1}) ejected along the poles, and neutron-rich material of lower entropy (i.e., $\sim$15 k_B baryon^{-1}) at mid-latitudes. Here, the electron fraction is clustered around a neutron-rich mean, with $Y_e = 0.25$ and an entropy of $\sim$8 k_B baryon^{-1}. We illustrate these results in Figure 7 with histograms for the electron fraction and entropy distributions of the ejecta material. Given the $\sim$0.1 $M_\odot$ of material expelled in the B12 model with such characteristics, these yields may have some significance for the composition of the interstellar medium in *r*-process nuclei (see § 4.2), as suggested by Wheeler et al. (1998).

The long-term development of the explosion is influenced by the early excavation of the polar regions of the white dwarf. Hence, the explosion remains confined to the poles, extending only down to a $\sim$40° latitude. Some fraction of the material on

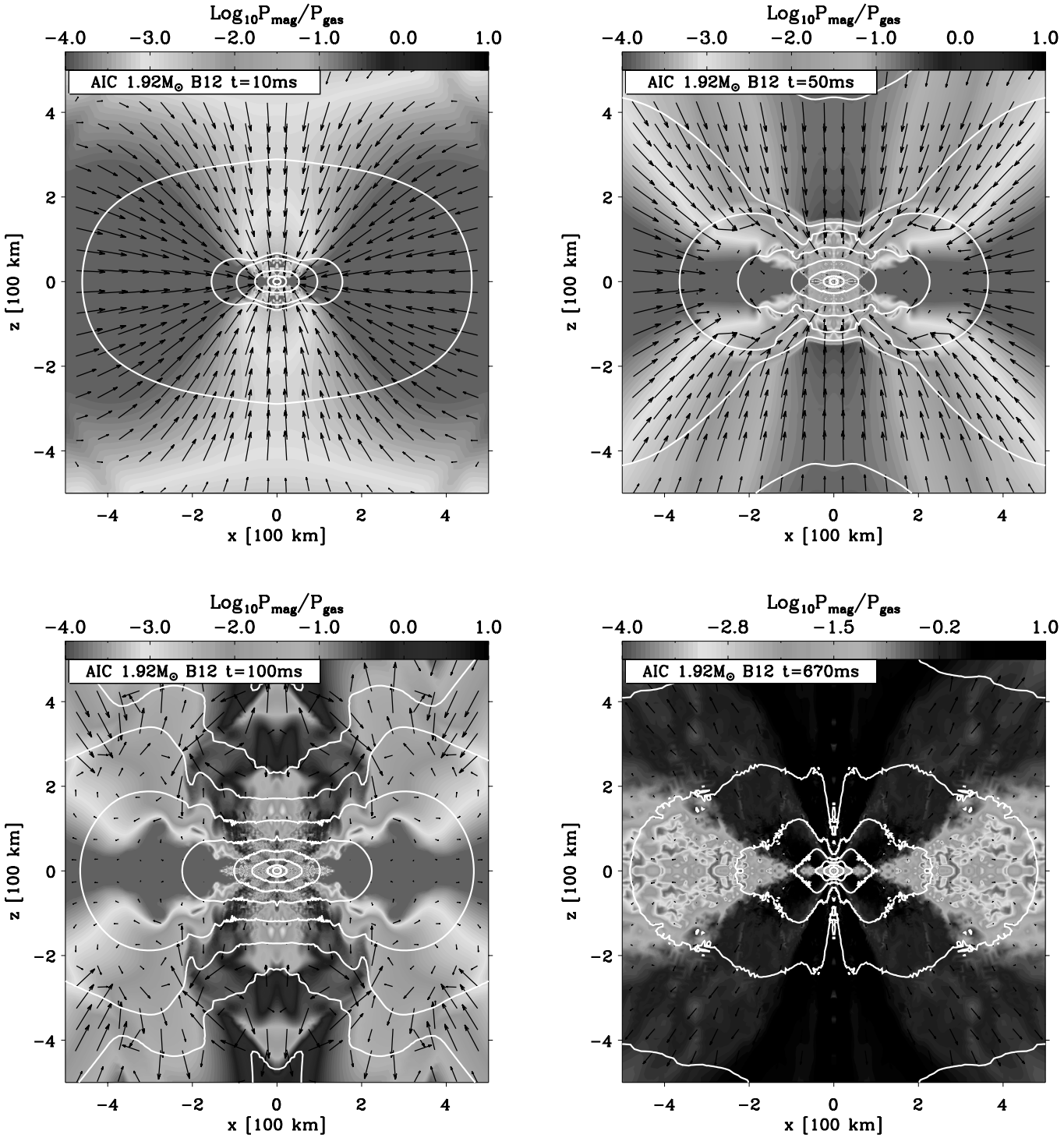

FIG. 5.—Color map of the logarithm of the ratio of magnetic pressure to gas pressure for the B12 model, at 10 ms (*top left*), 50 ms (*top right*), 100 ms (*bottom left*), and 670 ms (*bottom right*) after bounce, using white isodensity contours starting at 10^{14} g cm^{-3} shown for every decade in density, as well as black vectors to represent the velocity, saturated at a length of 7% of the width of the display for a magnitude of 5000 km s^{-1} [*See the electronic edition of the Journal for a color version of this figure.*].

the polar-facing side of the excavated white dwarf is entrained by the ejecta, the velocity shear at the interface inducing Kelvin-Helmholtz rolls that mix low and high Y_e material (the lower resolution of our simulations in the region of interest, around a few hundred kilometers, underresolves this instability, but some rolls are clearly seen). At the end of the simulation, this interface has visibly been eroded, and the lobes of the white dwarf progenitor subtend a smaller opening angle (compare the left and right panels in the top row of Fig. 1). Interestingly, most of this entrained material does not reach the escape speed from this AIC progenitor, of the order of 15,000 km s^{-1}, and ultimately remains bound to the system. In practice, its trajectory curves back toward the equatorial plane, which it hits at a radius of 2000–3000 km from the PNS. Hence, material with low Y_e is being fed into the

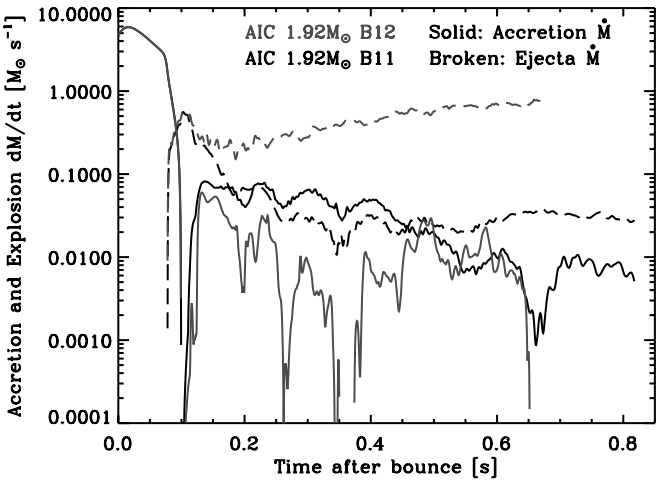

FIG. 6.—Time evolution for the B11 (*black*) and B12 (*red*) models of the instantaneous integrated mass flux accreting (*solid lines*) or outflowing (*dashed lines*) through a shell at a radius of 500 km. (See text for discussion.) [*See the electronic edition of the Journal for a color version of this figure.*]

backside of the disk, from regions that were originally near the pole.[6] If the explosion persists over a long time, such ablation may completely erode and destroy the original lobes of the progenitor white dwarf, although perhaps it may merely redistribute this material to larger distances still within the white dwarf potential well. Material located beyond a distance of $\sim$1000 km from the PNS and above a $\sim 40^{\circ}$ latitude follows an essentially radial, ballistic trajectory and escapes the gravitational potential of the massive white dwarf.

At the end of both simulations, the neutron stars have a strongly oblate structure and fast rotation (see also the comparable equilibrium configurations of Liu & Lindblom 2001). Although the pole-to-equator radius contrast is essentially preserved, in the B12 model the 10^{10} g cm^{-3} isodensity contour, for example, is stretched out to $\sim$100 km at midlatitudes, and to only $\sim$50 km in the B11 model (compare the contour morphology in the left and right bottom panels of Fig. 1). The same holds for the temperature, which remains large along the pole even at 100 km ($\sim$3 MeV in the B12 model compared with $\sim$1 MeV in the B11 model). Higher magnetic fields modify the hydrostatic configuration of the neutron star, leading to its spatial extension, and the subsequent peeling back of the corresponding regions by the magnetically driven wind.

The postbounce neutrino signals of the AIC of the 1.92 $M_{\odot}$ white dwarf we have modeled (Fig. 8) are strongly latitude-dependent,[7] with a systematic increase (irrespective of neutrino type) by up to a factor of 2 from the equatorial to the polar directions (D06). The gravity-darkened fast-rotating PNS has a much lower temperature along the equator, which inhibits the emission, essentially thermal, of "ν_{μ}" neutrinos, and the flatter density profile along the equator modifies capture rates. The enhancement in neutrino luminosity at higher latitudes, whatever the species, is a purely geometrical effect and results from the increased subtended angle occupied by the PNS for viewing angles at higher latitudes (see also Walder et al. 2005). Irrespective of the energy group and the neutrino species, the corresponding "radiating" neutrinosphere is oblate and occupies the largest solid angle for observers along the poles (see D06 for further discussion on this latitudinal variation of neutrino fluxes). In addition, we note that, for a given time after bounce, the electron neutrino luminosity is reduced in the B12 model compared to the B11 model, by $\sim$30% along the equator and $\sim$40% along the pole, while the luminosities associated with the $\bar{\nu}_e$ and "ν_{μ}" neutrinos match their counterparts in the two models within a few percent. Note that, provided it is not later ejected, the delayed mass accretion, over viscous timescales (see § 4.3), of the lobes of the progenitor white dwarf has the potential to power the neutrino luminosity at a low level over a longer time than would typically obtain for isolated neutron stars.

4. DISCUSSION

4.1. *Magnetic Effects*

The previous section highlighted the main features and phases of the AIC of white dwarfs, for both weak and strong magnetic fields. The main effect of magnetic fields is to trigger a much more powerful explosion, here reaching $\sim$1 B after just 300 ms after bounce, tapping some free energy of rotation of the PNS, and ejecting mass at a rate of a few $\times 0.1$ of $M_{\odot}$ s^{-1}. We thus find that if magnetic pressure becomes comparable to gas pressure at the neutron star surface, a magnetically driven wind is initiated whose properties are boosted when compared to the pure neutrino-driven wind case (i.e., with weak or negligible magnetic field), the latter with mass-loss rates of a few $\times 0.001$ $M_{\odot}$ s^{-1} and global ejecta energies of at most $\sim$0.1 B. Note, in particular, that the free energy of rotation is also available at the same level in the weak magnetic field case (model B11); it is only that the means to extract it are insufficient. Magnetically aided, the explosion is sustained at a much higher level, rendering the neutrino component subdominant (Fig. 2).

The magnetic contribution to the pressure balance at a few tens of kilometers can be significant and can deform the PNS compared to the weak-field case, sphericizing the isodensity contours (see, e.g., the bottom panels of Fig. 1). The energy to amplify the magnetic field, to puff up the neutron star (although mostly along the poles), and to drive a more powerful explosion stems from the tapping of core rotational energy (where it is the most abundant), which is also manifest in the spin-down of the core, in analogy with the extraction of angular momentum in accretion disks (Blandford & Payne 1982). By $\sim$500 ms after bounce, the average PNS period[8] is 30% larger in the high magnetic field case, and is $\sim$20 ms.

4.2. *Nucleosynthetic Yields*

Guided by the results of Hillebrandt et al. (1984), Wheeler et al. (1998) suggested promptly exploding ONeMg cores as the production sites of *r*-process nuclei, given the low electron fraction ($Y_e \sim 0.2$) and the low entropy of their ejecta ($S \sim 15 k_{\rm B}$ baryon^{-1}; see also Qian & Woosley 1996; Hoffman et al. 1997). However, radiation hydrodynamics simulations of the collapse of Fe or

[6] Note that, initially, in our Eulerian approach, we fill the ambient medium around the progenitor white dwarf with low-density, low-temperature material, which nonetheless may do work against the ejecta expansion and lead to the fallback of some material at the outskirts of the disk. At the start of the simulation, this ambient pressure $P_{\rm ambient}$ is about 8×10^{19} dyne cm^{-2}, over 4 orders of magnitude smaller than the pressure in the surface layers of the white dwarf. The *PdV* work done by the ejecta to expel this ambient material translates into an energy penalty on the order of $P_{\rm ambient} \times (\frac{4}{3}\pi R_{\rm max}^3 - \pi R_{\rm eq}^2 \times 2R_{\rm pol}) \sim 2 \times 10^{46}$ erg, where $R_{\rm max}$ is the maximum radius of the grid, and $R_{\rm eq}$ and $R_{\rm pol}$ are the equatorial and polar radii of the progenitor white dwarf. This energy penalty is small in comparison with the final energy of the explosion.

[7] Note that there was little neutrino field anisotropy for the 1.46 $M_{\odot}$ model described in D06, due to the more spherical shape of the newly formed neutron star.

[8] The average PNS period is computed assuming solid-body rotation for the same angular momentum budget in the PNS, with densities greater than 10^{10} g cm^{-3}.

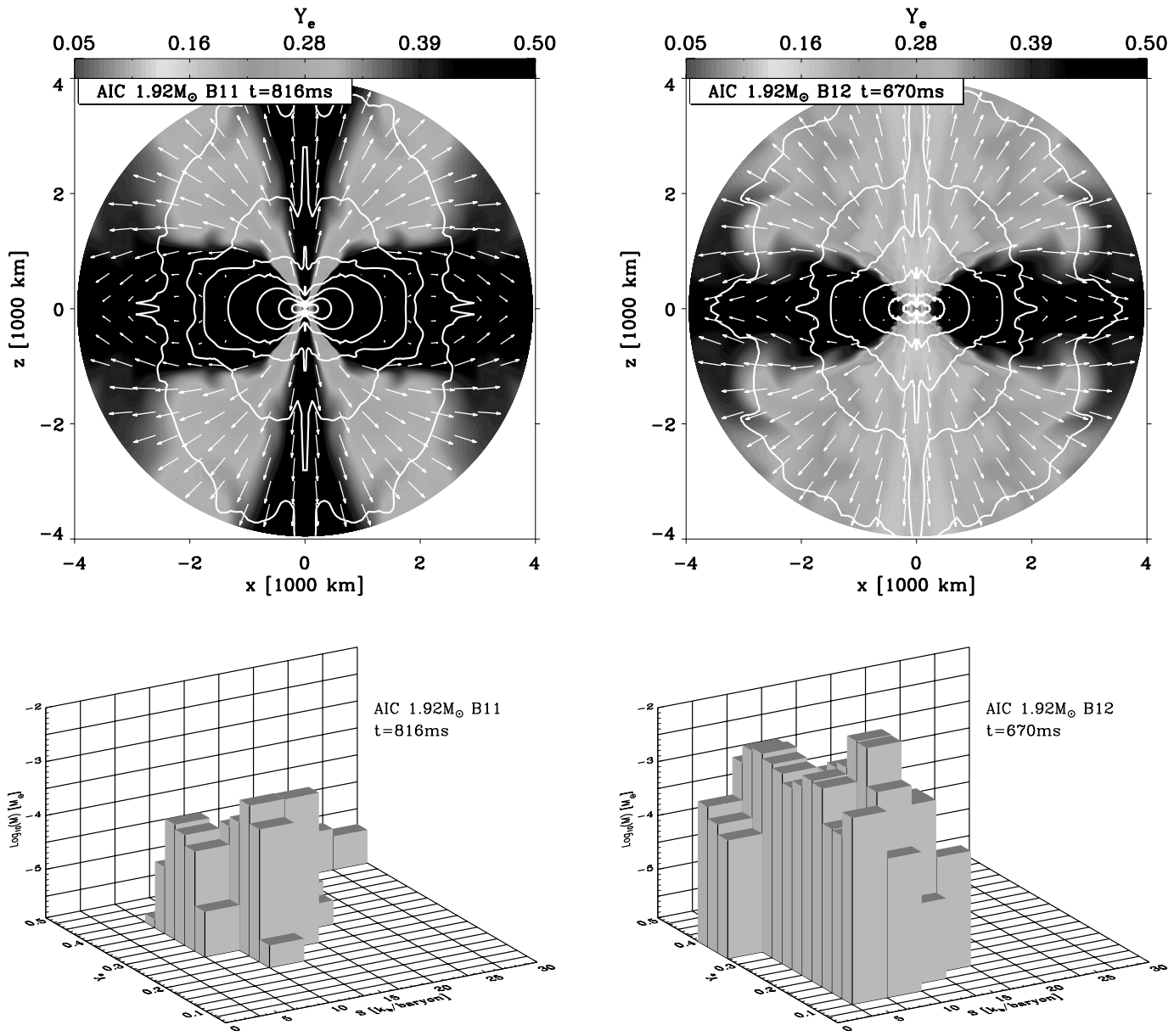

FIG. 7.—*Top*: Color map of the electron fraction Y_e at the end of the simulation for model B11 (*left*) and model B12 (*right*), with white isodensity contours for the density shown every decade starting at 10^{10} g cm^{-3}, and white velocity contours saturated at 7% of the width of the display for a magnitude of 10,000 km s^{-1}. *Bottom*: Three-dimensional histogram of the distribution of the ejecta mass as a function of electron fraction, Y_e, and entropy, S, for the B11 (*left*) and B12 (*right*) models. Note the larger total ejecta mass, and the stretching of the electron fraction distribution to values as low as 0.1, in the B12 model. (See text for discussion.) [*See the electronic edition of the Journal for a color version of this figure*.]

ONeMg cores demonstrated that the explosion can never be prompt (can never be on timescales of a few milliseconds) and that, instead, the shock stalls. Eventually, in the context of the ONeMg cores of low-mass massive stars or AICs, the stalled shock overcomes accretion, because of the extremely steep density gradient above the core (Kitaura et al. 2006; D06; Burrows et al. 2007b, 2007c).

The results of our present simulations confirm that there is no prompt explosion in the AIC of white dwarfs and that, indeed, ejecta with low electron fraction are produced. At low magnetic field, the ejecta are primarily at Y_e values between 0.25 and 0.5, but with a total mass of a few $\times 0.001\ M_\odot$ (see Fig. 7). At high magnetic fields, the distribution is somewhat altered, with no material at entropies larger than $\sim 15 k_B$ baryon^{-1}, and ejecta electron fractions extending down to $\sim$0.1. More importantly, the total ejecta mass is a factor of $\sim$40 larger than in the B11 model and renders such distributions of interest. At the end of the B12 simulation, we find a total ejecta mass of 0.15 $M_\odot$, with 0.1 $M_\odot$ of the material with Y_e between 0.1 and 0.2. and an entropy of $S \sim 10 k_B$ baryon^{-1}. Following the argument of Wheeler et al. (1998), in reference to Hoffman et al. (1997), this indicates the production of nuclei with an atomic mass of up to 190 and motivates further investigation of *r*-process nucleosynthesis under such conditions.

Woosley & Baron (1992) and Fryer et al. (1999) used the nucleosynthetic yields of AICs to estimate their occurrence rate. Based on constraints set by a number of isotopic abundances (e.g., ^{62}Ni, ^{88}Sr; see Woosley & Hoffman 1992), Hartmann et al. (1985) suggested that less than $10^{-5}\ M_\odot$ of material with an electron fraction below 0.4 can be ejected per supernova event. By the end of the B11 (B12) simulation, a total of $\sim$0.004 $M_\odot$ ($\sim$0.15 $M_\odot$) of such low-Y_e material has been ejected (note

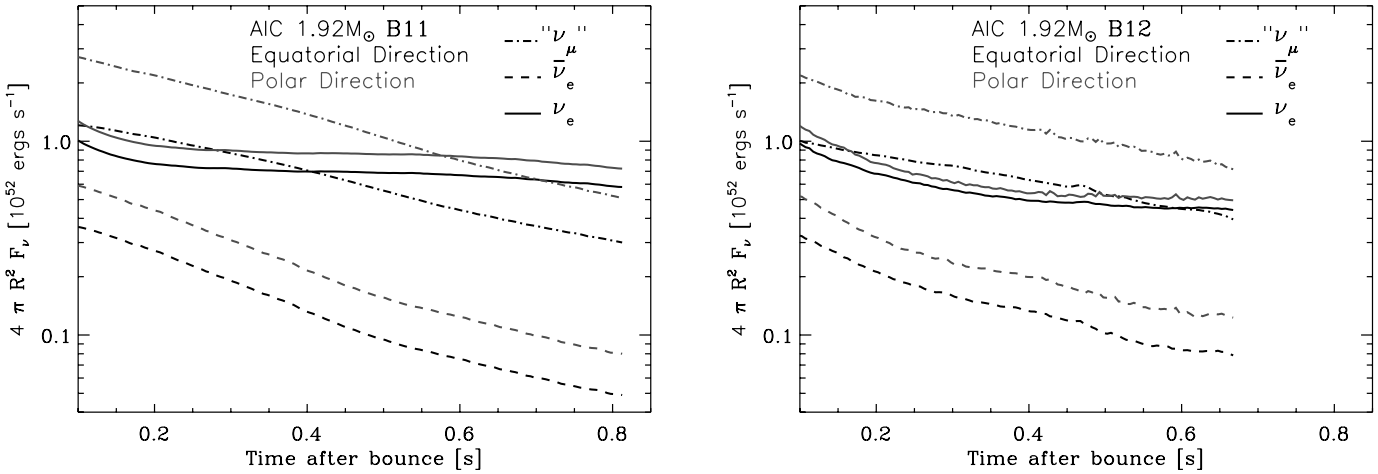

FIG. 8.—*Left*: Time evolution of the electron neutrino (*solid line*), antielectron neutrino (*dashed line*), and "ν_μ" neutrino luminosity (*dash-dotted line*) along the equatorial (*black*) and polar (*red*) directions, for model B11, at $R = 400$ km, and starting 100 ms after bounce. Here, neutrino luminosities are integrated over neutrino energy, and correspond to the quantity $4\pi R^2 F_\nu(t, R, \theta)$, adopting the flux along the polar direction ($\theta = 0$) or along the equatorial direction ($\theta = 90°$). *Right*: Same as left, but for model B12. Note the systematic reduction of all neutrino fluxes along the equatorial direction (neutrinos fluxes decrease in a continuous fashion toward lower latitudes), an effect that is essentially geometrical and stems from the larger angle subtended by the PNS as seen from higher latitudes. This effect is primarily caused by the fast rotation of the PNS, rather than its magnetic properties. Notice also that, for a given time after bounce, the electron neutrino luminosity is reduced in the B12 model, and that the antielectron neutrino and "ν_μ" neutrino luminosities remain comparable to their B11-model counterparts. (See text for discussion.) [*See the electronic edition of the Journal for a color version of this figure*.]

that this includes material that has left the grid, the maximum computational radius being only 4000 km), which, together with the isotopic constraints, sets the rate to a maximum of $\sim 5 \times 10^{-5}$ yr^{-1} for B11-type events, and $\sim 1.3 \times 10^{-6}$ yr^{-1} for B12-type events.

Following Woosley & Baron (1992), an alternate constraint can be imposed by using the solar ratio of the oxygen to the ^{88}Sr abundance, assuming oxygen is contributed primarily by core-collapse explosions of massive-star progenitors, and ^{88}Sr primarily from AICs. For the B11 simulation, material with a Y_e between 0.4 and 0.45 is ejected with a very small cumulative mass of $\sim 5 \times 10^{-5}\ M_\odot$ at 800 ms after bounce, corresponding to a rate constraint of 0.02 yr^{-1}. In the B12 simulation, more mass is expelled in total, but no ejecta have an electron fraction above 0.4 after $\sim$200 ms after bounce, and we indeed find a total ejected mass with an electron fraction between 0.4 and 0.45 that is comparable to that of the B11 simulation, and a rate of $\sim$0.02 yr^{-1}. Hence, the second constraint set by the oxygen and ^{88}Sr solar abundances is not really relevant for the AIC we simulate, since we predict nearly all of the nuclei ejected have an electron fraction below 0.4. Overall, if the neutrino- or magnetically driven winds we witness in the B11 and B12 simulations persist over a number of seconds, the corresponding Galactic AIC rate, as limited by nucleosynthetic yields, should be at most[9] 10^{-6} yr^{-1}, thus from a factor of a few to up to 2 orders of magnitude lower than that obtained in the simulations of Woosley & Baron (1992) or Fryer et al. (1999). Our B12 simulation suggests that if the progenitor core of such AICs rotates quickly and significant magnetic field amplification occurs after PNS formation, the event rate of the AIC of white dwarfs is doomed to be very small, of the order of 10^{-6} yr^{-1}, less than 4 orders of magnitude lower than the event rate of massive star explosions.

We observe a strong pole-to-equator variation of all neutrino fluxes in both the B11 and the B12 models. This property was discussed in D06 and is linked to the fast rotation and oblateness of the PNS (see also Walder et al. 2005). Here, we find that this anisotropy persists with the introduction of magnetic fields. Moreover, although the antielectron neutrino and the "ν_μ" neutrino fluxes remain comparable in both the B11 and B12 models, we find that the electron neutrino flux is systematically lower in the B12 model (for a given direction).

4.3. *Are AICs GRB/X-Ray Flash Progenitors?*

The AIC of a white dwarf has been proposed repeatedly as a potential GRB progenitor (Usov 1992, 1994; Dar et al. 1992; Yi & Blackman 1997, 1998; Dai & Lu 1998). The attractiveness of such collapsed white dwarfs stems partly from (1) the absence of a progenitor envelope, preventing the choking of possibly relativistic ejecta launched at the surface of the newly formed neutron star, and (2) an inherently large angular momentum that may be insufficient in massive star progenitors to meet the conditions necessary for the collapsar model (Woosley 1993; MacFadyen & Woosley 1999).

Usov (1992, 1994) invoked the generation of a relativistic electron-positron plasma from such a fast-rotating highly magnetized neutron star, powered over a timescale of seconds, leading to the emission of X-rays and γ-rays at the wind photosphere. A similar model was proposed by Yi & Blackman (1997, 1998) and Dai & Lu (1998), in which a magnetized millisecond pulsar powers a fireball by magnetic dipole radiation. Alternatively, Dar et al. (1992) suggested that electron-positron pair production from neutrino-antineutrino annihilation outside the PNS would trigger a GRB, provided the neutron star environment is not polluted with more than $3 \times 10^{-4}\ M_\odot$ of baryons.

In the context of standard core-collapse supernova explosions, neutrino-antineutrino annihilation does not lead to appreciable net energy gain for the wind or ejecta, because the energy tends to be deposited deep in the PNS, or at best in the cooling region in the vicinity of the neutrinosphere, thereby contributing negligibly to the supernova explosion (Cooperstein et al. 1987). In addition, the annihilation cross section is strongly enhanced for large-angle collisions, favoring nonspherical configurations such as disks or tori (Janka 1991; Ruffert et al. 1997). The disklike morphology of the neutron stars formed in the AIC of white

[9] It is unclear how quickly the mass-loss rate in the B12 model is going to decrease over the next few seconds, as it must, and consequently the corresponding cumulative mass loss cannot yet be accurately determined.

dwarfs, and the additional pinching of isodensity contours in the polar regions, seems to offer an interesting prospect. Following the method of Ruffert et al. (1997) and using the final configuration of the B12 model, we estimate an ν_e-$\bar{\nu}_e$ annihilation power of 0.01 B s^{-1}, deposited primarily along the polar direction, but within 20–50 km of the PNS center. This is a rough estimate, but it suggests that if our B11/B12 models are sensible representations of the AIC of white dwarfs, then little can be gained from neutrino-antineutrino annihilation, in particular in comparison with the power injected by magnetic means. This is the case at a few hundred milliseconds after bounce, but it may change at later times of many seconds.

In the general context of core-collapse supernovae, Tan et al. (2001) investigated the acceleration to relativistic speeds of the surface layers of the progenitor as the shock, generated at bounce, breaks out. The AIC of white dwarfs presents an interesting context for such an effect, given the absence of a progenitor envelope. But the explosion energies and the ejecta masses reported in the spherical simulations of the AIC of white dwarfs (Woosley & Baron 1992; Fryer et al. 1999) were low, and Tan et al. confirmed the conclusion of those authors that the AIC of white dwarfs cannot lead to any sizable γ-ray emission or relativistic ejecta. In D06, and reproduced here as well for the B11 model, the explosion is strongly underenergetic for weak magnetic fields (reaching only $\sim$0.1 B after about 500 ms, with a power that has stabilized to $\sim$0.1 B s^{-1} and that may be sustained for a few seconds). Most of the power is in the form of a neutrino-driven wind, with an associated mass-loss rate of a few $\times 0.001\ M_\odot$ s^{-1}. The original blast that breaks out of the polar caps of the progenitor white dwarf would represent the best option in the context of the Tan et al. study, but the shock, debilitated by neutrino losses and the photodissociation of nuclei, stalls only mildly. It is not re-energized by neutrino energy deposition. Rather, it breaks out of the white dwarf by virtue of the abrupt density gradient. The resulting early blast amounts to a mere 10^{-4} B, and despite the low baryon loading of the ejecta ($\sim 10^{-4}\ M_\odot$), they reach velocities of only 1/10 of the speed of light.[10] In model B12, the explosion energy goes above 1 B, but the wind mass-loss rate is commensurate with this energy gain, and is on the order of 0.1 $M_\odot$ s^{-1}. As a result, the production of a GRB via the Tan et al. scenario is again not viable. The asphericity of the explosion does not dramatically alter this conclusion, since, while the explosion energy is deposited in a smaller volume, the mass flux is also confined to a smaller opening angle and leads to higher effective baryon loading. The spherically symmetric, adiabatic, steady-state, LTE model of a super-Eddington wind by Paczynski (1990) supports the same conclusion. Given a rate of energy deposition of a 0.1–1 B s^{-1} and a mass-loss rate between a few $\times 0.001$ and $\sim$0.7 $M_\odot$ s^{-1} for the B11 and B12 models, respectively, the temperature at the photosphere would be vanishingly small in both cases, with a photon luminosity of at most 10^{40} erg s^{-1}. The baryon loading of the ejecta that occurs in the B12 model, associated with the magnetic driving of the wind, nulls the benefit of the additional explosion power. The low photospheric temperature obtained here suggests that, since the ejecta become optically thin at such a late time, no radiation would be visible in the optical. The negligible amount of ejecta material with a Y_e of 0.5, which corresponds to radioactive ^{56}Ni, means that there is no energy source to counteract the strong adiabatic cooling of the neutrino- or magnetically driven wind. It seems that neutrinos and gravitational waves would be the only significant signatures of the explosion.

The AIC of a white dwarf might give birth to a magnetar, following magnetic field compression and amplification in the fast-rotating neutron star. Yi & Blackman (1997, 1998), and Dai & Lu (1998) suggested that such magnetars could, through extraction of rotational energy, power Poynting flux dominated ejecta and lead to GRBs at cosmological distances. Indeed, during the cooling phase of such fast-spinning highly magnetized neutron stars, the millisecond protomagnetar wind may transition from nonrelativistic and thermally driven to magneto-centrifugally driven, and finally to relativistic and Poynting flux dominated (Thompson et al. 2004; Bucciantini et al. 2006; Metzger et al. 2007; Thompson 2007). This scenario in fact has the potential to make the AIC of white dwarfs detectable in the γ-ray range. Furthermore, based on the local universe distribution of short-hard GRBs among all galaxy types, rather than exclusively with young stellar populations, Chapman et al. (2006) have proposed the AIC of white dwarfs as an alternative to massive star progenitors for the formation of magnetars, whose soft γ-ray emission is associated with giant flaring events. We concur in principle with this proposition, although the AIC rate of at most $\sim 10^{-6}$ yr^{-1} for B12-type events that we infer in § 4.2 suggests that magnetars originating from the AIC of a fast-rotating white dwarf should be significantly underrepresented in the magnetar population.

An AIC analog to the collapsar model (Woosley 1993; MacFadyen & Woosley 1999) is an obvious alternative, with both the transition of the PNS to a black hole and energy deposition in the excavated polar regions at a high rate of a few $\times 0.1$ B s^{-1}. In the context of the AIC of white dwarfs, the potential for formation of a black hole seems uncertain, as it might be difficult in nature to ultimately meet the basic mass requirement of a 2–2.5 $M_\odot$ (baryonic) neutron star for black hole formation (Baym et al. 1971; Arnett & Bowers 1977). In D06, we studied two models, with 1.46 and 1.92 $M_\odot$ masses. The PNS mass was larger in the lower mass progenitor, because in the 1.92 $M_\odot$ model much of the mass ended in a massive disk. Higher mass AIC progenitors would need even more angular momentum to achieve a stable equilibrium configuration, which would likely result in the formation of even higher mass disks on extended quasi-Keplerian orbits. At the same time, magnetic stresses at the surface of the neutron star lead to such high mass-loss rates that the PNS mass paradoxically decreases with time (the PNS mass in the B12 model decreases to $\sim$1.3 $M_\odot$ at $\sim$500 ms after bounce). It thus seems that accretion, leading to black hole formation, would have to operate over a very extended time, and it is not clear, given the explosion power that can be obtained (witness the results for the B12 model), whether accretion will ever win against explosion. A further obstacle to high accretion rates in the AICs is the extended configuration of the mass distribution outside the neutron star, with progenitor lobes located at $\sim$1000 km, rather than around $\sim$100 km in the ideal setup for the collapsar model (Woosley 1993; MacFadyen & Woosley 1999). The outcome here is closely related to the original mass distribution of the white dwarf at the time of collapse. Current SPH simulations of coalescing white dwarfs, one formation channel of AICs, suggest that a significant fraction of that material goes into a Keplerian disk, loosely bound, and thus not directly involved in the collapse/bounce of the core, nor with the subsequent explosion. This material may represent a substantial amount of mass, perhaps up to 1 $M_\odot$, but is located at least at 1000 km away from the neutron star or would-be black hole, so that the actual accretion rate is very small. In the configuration of

[10] Note here that the low-density ambient medium surrounding the progenitor white dwarf may be slightly inhibiting further acceleration, but Fig. 11 of Tan et al. (2001) suggests that this shock breakout is in any case symptomatically underenergetic.

the 1.92 $M_\odot$ model described here, we have 0.5 $M_\odot$ available in the disk, with an associated viscous accretion timescale of $\sim$100 s (using an α parameter of 0.1; Shakura & Sunyaev 1973), and hence a feeble accretion rate of 5×10^{-3} $M_\odot$ s^{-1}. This is a factor of 100 lower than the minimum value quoted in the context of the collapsar model. This extended configuration for AICs is in fact reminiscent of the fallback scenario of Rosswog (2007) for double neutron star mergers, in which material is placed on eccentric orbits during the merger event. Note that, here again, accretion onto a black hole is a prerequisite for the powering of a relativistic jet, and ultimately γ-ray radiation. In the context of AIC, such accretion may simply extend the PNS wind phase over a longer period, and not lead to the formation of a black hole.

4.4. *Ultimate Fate of the AIC of White Dwarfs*

The AIC of white dwarfs seems very unfavorable as a progenitor of γ-ray, or even optical bursts, and direct detection of such events might instead come from neutrino or gravitational wave detectors (see §§ 3 and 10 of D06). Indirectly, we may infer their existence through the *r*-process nuclei ejected during the explosion (§ 4.2).

Another avenue is to search for them in the neutron star population. Fallback following SN explosions of massive progenitors is expected to bury the PNS and weaken its surface magnetic field,[11] as in magnetic neutron stars accreting from a companion star (see, e.g., Geppert & Urpin 1994; Payne & Melatos 2004, 2007). This argument would suggest that magnetic neutron stars may originate from the AIC of white dwarfs, since these are exempt from such fallback. Observations of magnetic neutron stars in binary systems have indeed been interpreted in this way (see, e.g., Taam & van den Heuvel 1986; Ergma 1993; van den Heuvel & Bitzaraki 1995; van Paradijs et al. 1997), although our simulations suggest that some "fallback," albeit modest, could occur from the progenitor lobes of the white dwarf and bury the large surface fields of $\sim 10^{15}$G that we see in the B12 model a few hundred milliseconds after bounce. Hence, in this context, whether additional material from the progenitor lobes of the white dwarf accretes onto the highly magnetized PNS may determine whether it will retain its magnetar-like fields or transition to a weaker field pulsar. Despite the extraction of angular momentum by magnetic fields, the PNS remains a millisecond-period rotator. Further accretion from the Keplerian disk would mitigate the loss of angular momentum, and thus AICs of white dwarfs should consistently lead to rapidly rotating pulsars after this original phase. On longer timescales of hours or days, however, magnetic torquing may be more in evidence and may spin down the PNS as it transitions to a magnetar-like object. In this case, the remnant could be a highly magnetized object, with a much reduced rotation rate, a correlation that has been found in the pulsar population (Vranevsevic et al. 2006). Interestingly, if such accretion is not significant, this material could be found in a debris disk, as recently observed around an isolated neutron star (Wang et al. 2006).

Finally, we reported in D06 that in the simulation for the 1.46 $M_\odot$ AIC model of Yoon & Langer (2005), carried over 180° (i.e., including both hemispheres), perfect north-south symmetry was preserved. We have used this observation to carry out all subsequent investigations in a 90° quadrant, thus in just one hemisphere. We expect that the AIC of white dwarfs leads to essentially perfect north-south symmetry, a property that applies more generally to the explosion following the collapse of ONeMg cores, universally characterized by a steep density profile above the core. Consequently, these explosions should involve no significant kick to the PNS. This supports the notion that the AIC of white dwarfs can, at least theoretically, contribute to the neutron star population of globular clusters (see, e.g., Bailyn & Grindlay 1990; Ivanova et al. 2006). But given the very low inferred rates of AICs (in particular for the B12-like events), the ONeMg cores of low-mass massive stars are more likely candidates. Similarly, this also supports the association of collapsed ONeMg cores with the populations of low-velocity, low-mass neutron stars found in low-eccentricity double neutron star systems (see, e.g., van den Heuvel 2007).

5. CONCLUSION

We have presented multigroup, flux-limited diffusion, magnetohydrodynamics simulations of the accretion-induced collapse (AIC) of white dwarfs, focusing on the 1.92 $M_\odot$ model of Yoon & Langer (2005). The main incentives were to gauge the relevance and estimate the magnitude of MHD effects in such collapse events, and thereby to address a potential limitation of the simulations in D06. The key *Ansatz* in the present work is that, although the magnetic field distribution and magnitude in the progenitor white dwarf are unknown, fast and differential rotation in the collapsed object is expected to lead to an exponential amplification of any initially weak poloidal field through the magnetorotational instability, reaching large values at saturation. In this context, the magnitude of the postbounce MHD effects we report from our simulations will thus be determined, in a more physical sense, by the angular momentum budget rather than by the initial field in the precollapse white dwarf. Provided angular momentum is abundant, we find that MHD effects lead to large quantitative changes when compared with an equivalent situation ignoring magnetic fields. Said differently and in a broader sense, we expect significant MHD effects in core-collapse events with fast rotation, effects that cannot be ignored without compromising the conclusions.[12]

Perhaps the most striking property of the AIC of a 1.92 $M_\odot$ white dwarf model with large initial magnetic fields is that the explosion energy at just a few hundred milliseconds after bounce is no longer an anemic 0.01 B, but is on the order of 1 Bethe, with an ejecta mass raised from a few $\times 0.001$ to $\sim$0.1 $M_\odot$. Significant rotational energy is extracted from the core with the inclusion of magnetic fields, directly seen in the decrease in rotational energy and the spin-down of the PNS. This energy is transformed into magnetic energy that powers the explosion. For higher B fields, the density distribution at the surface of the neutron star is more spherical, the 10^{10} and 10^{11} g cm^{-3} density contours stretching further out along the pole, aided by magnetic stresses. We find that mass loading of the ejecta is so severe that no relativistic high-energy electromagnetic transient can be expected during the PNS phase. In the past, the AIC of white dwarfs has been invoked as a potential GRB progenitor, but this was usually done in ignorance of the neutrino-driven wind that prevails during the first tens of seconds after the formation of the PNS. MHD effects seem to make this situation even worse, not better, by loading magnetically driven ejecta with 100 times more baryons.

[11] In this context, the mass accreted after a delay starts with a very weak initial field. Little compression ensues and the spin-up is moderate, so that, despite the presence of velocity shear in the region of accretion, we expect only modest field amplification.

[12] Nonaxisymmetric instabilities of such fast-rotating white dwarfs may alter the angular momentum distribution after bounce (Ott et al. 2007), with the potential to modify magnetic field amplification rate as well as the accretion rate we observe in our simulations. Numerical simulations of the kind presented here, but in 3D, are needed to quantify these effects.

In the single-degenerate formation scenario, magnetic torques operating over evolutionary timescales might force the white dwarf into solid-body (and, perhaps, critical) rotation, and prevent its growth much beyond the canonical Chandrasekhar mass, thus preventing a transition to a black hole after PNS formation. However, in the double-degenerate scenario, differential and fast rotation results after the merging event and a super-Chandrasekhar white dwarf may form. Ultimately, transition to a black hole may occur if the total PNS mass exceeds the general-relativistic limit for gravitational stability. The transition to a black hole, by shutting off the wind from the PNS, may then lead to a γ-ray burst or an X-ray flash, but the 2–2.5 $M_\odot$ mass limit for black hole formation restricts the number of adequate AIC progenitors to a very small number, difficult to estimate, but perhaps to 1 in 100 AICs. The coalescence of two white dwarfs[13] seems the more favorable configuration, but no more than a few $\times 0.1\ M_\odot$ of material placed at large distances (a few 1000 km) would be available for accretion, and this over a viscous timescale of $\sim$100 s, and thus with a feeble accretion rate of at most $5 \times 10^{-3}\ M_\odot\ \mathrm{s}^{-1}$. In the unlikely event that all these necessary conditions were met, the relativistic beaming (with opening angle θ_j) of the radiating ejecta would decrease the probability of γ-ray detection by a factor $0.5(1 - \cos\theta_j)$, i.e., 2–3 orders of magnitude for a 5°–15° opening angle.[14] Together with the constraints from nucleosynthetic yields of B12-like events, the 1 in 100 AICs that may reach the black hole mass limit, and the inherent beaming of the resulting γ-ray radiation, we estimate the detection rate of γ-ray bursts associated with AICs to be on the order of $10^{-10}\ \mathrm{yr}^{-1}$, significantly lower than the average rate per galaxy of $4 \times 10^{-7}\ \mathrm{yr}^{-1}$ inferred from GRBs detected with BATSE (Zhang & Mészáros 2004).

Moreover, the absence of nickel in the ejecta precludes any significant optical signature for the event, which should thus remain obscure at all wavelengths. If the AIC occurs in our Galaxy, possible signatures should instead be from the neutrino burst that accompanies the formation and the cooling of the PNS, and gravitational waves from the very aspherical bounce and the anisotropic neutrino emission (Ott 2007).

The AIC of white dwarfs may, however, have a significant impact on the interstellar medium composition in *r*-process nuclei. We find that the AIC of rapidly rotating white dwarfs leads to explosions that eject copious amounts of neutron-rich material, with an electron fraction reaching down to $\sim$0.1–0.2, depending on the magnitude of the neutrino/antineutrino absorption by the ejecta. If not magnetically aided, the neutrino-driven wind leads, however, to a low ejecta mass of a few $\times 0.001\ M_\odot$, which, given the low occurrence rates for AIC, makes these yields somewhat irrelevant. If magnetically aided, as in the simulation B12 presented here, about 0.1 $M_\odot$ of material is ejected with an electron fraction between 0.1 and 0.2, making the AIC of white dwarfs a possible *r*-process site, as promoted in an analogous context by Wheeler et al. (1998). More importantly, constraints placed by solar isotopic abundances require that such pollution of the interstellar medium by magnetically driven winds of AICs occurs with an event rate of at most $\sim 10^{-6}\ \mathrm{yr}^{-1}$. If we believe the context adopted for this work, this suggests that the circumstances leading to such fast-rotating white dwarfs are rare.

An important ramification of this work is that, free of significant fallback, the AIC of white dwarfs offers a possible scenario for the formation of highly magnetized neutron stars, potentially with magnetar-like surface fields of 10^{15} G, with magnetically torqued cores that spin down over many seconds. Here again, however, the low event rate of such AICs should result in their contributing only modestly to the magnetar population.

We thank Jim Liebert, Jeremiah Murphy, Martin Pessah, Todd Thompson, and Stan Woosley for fruitful discussions and their insight. We acknowledge support for this work from the Scientific Discovery through Advanced Computing (SciDAC) program of the DOE, under grant numbers DE-FC02-01ER41184 and DE-FC02-06ER41452, and from the NSF under grant AST-0504947. E. L. thanks the Israel Science Foundation for support under grant 805/04, and C. D. O. thanks the Joint Institute for Nuclear Astrophysics (JINA) for support under NSF grant PHY0216783. This research used resources of the National Energy Research Scientific Computing Center, which is supported by the Office of Science of the US Department of Energy under Contract DE-AC03-76SF00098.

[13] It even seems that these two white dwarfs would have to have comparable masses. Otherwise, the secondary would likely get disrupted, with its matter dispersed in a disk around the primary, rather than merging with the primary (Guerrero et al. 2004).

[14] This relativistic beaming of γ-ray radiation is inferred from the achromatic steepening breaks of some GRB optical afterglow light curves (Kulkarni et al. 1999; Harrison et al. 1999).

REFERENCES

Arnett, W. D., & Bowers, R. L. 1977, ApJS, 33, 415
Bailyn, C. D., & Grindlay, J. E. 1990, ApJ, 353, 159
Balbus, S. A., & Hawley, J. F. 1991, ApJ, 376, 214
Baron, E., Cooperstein, J., & Kahana, S. 1987a, ApJ, 320, 300
Baron, E., Cooperstein, J., Kahana, S., & Nomoto, K. 1987b, ApJ, 320, 304
Baym, G., Pethick, C., & Sutherland, P. 1971, ApJ, 170, 299
Belczynski, K., Bulik, T., & Ruiter, A. J. 2005, ApJ, 629, 915
Benz, W., Cameron, A. G. W., Press, W. H., & Bowers, R. L. 1990, ApJ, 348, 647
Berger, L., Koester, D., Napiwotzki, R., Reid, I. N., & Zuckerman, B. 2005, A&A, 444, 565
Blanc, G., et al. 2004, A&A, 423, 881
Blandford, R. D., & Payne, D. G. 1982, MNRAS, 199, 883
Blondin, J. M., Mezzacappa, A., & DeMarino, C. 2003, ApJ, 584, 971
Bucciantini, N., Thompson, T. A., Arons, J., Quataert, E., & Del Zanna, L. 2006, MNRAS, 368, 1717
Burrows, A., Dessart, L., Livne, E., Ott, C. D., & Murphy, J. 2007a, ApJ, 664, 416
———. 2007b, in AIP Conf. Proc. 937, Supernova 1987A: 20 Years After: Supernovae and Gamma-Ray Bursters, ed. S. Immler, K. W. Weiler, & R. McCray (New York: AIP), in press
Burrows, A., & Lattimer, J. M. 1986, ApJ, 307, 178
Burrows, A., Livne, E., Dessart, L., Ott, C. D., & Murphy, J. 2007c, ApJ, 655, 416
Chapman, R., Levan, A. J., Wynn, G. A., Davies, M. B., King, A. R., Priddey, R. S., & Tanvir, N. R. 2006, preprint (astro-ph/0610071)
Cooperstein, J., van den Horn, L. J., & Baron, E. 1987, ApJ, 321, L129
Dai, Z. G., & Lu, T. 1998, A&A, 333, L87
Dar, A., Kozlovsky, B. Z., Nussinov, S., & Ramaty, R. 1992, ApJ, 388, 164
Dessart, L., Burrows, A., Livne, E., & Ott, C. D. 2006a, ApJ, 645, 534
Dessart, L., Burrows, A., Ott, C. D., Livne, E., Yoon, S.-C., & Langer, N. 2006b, ApJ, 644, 1063 (D06)
Duncan, R. C., & Thompson, C. 1992, ApJ, 392, L9
Ergma, E. 1993, A&A, 273, L38
Etienne, Z. B., Liu, Y. T., & Shapiro, S. L. 2006, Phys. Rev. D, 74, 044030
Ferrario, L., & Wickramasinghe, D. T. 2005, MNRAS, 356, 615
Foglizzo, T., Scheck, L., & Janka, H.-T. 2006, ApJ, 652, 1436
Fryer, C., Benz, W., Herant, M., & Colgate, S. A. 1999, ApJ, 516, 892
Geppert, U., & Urpin, V. 1994, MNRAS, 271, 490
Gil-Pons, P., & García-Berro, E. 2001, A&A, 375, 87
Greggio, L. 2005, A&A, 441, 1055
Guerrero, J., García-Berro, E., & Isern, J. 2004, A&A, 413, 257
Gutierrez, J., Garcia-Berro, E., Iben, I. J., Isern, J., Labay, J., & Canal, R. 1996, ApJ, 459, 701

Hachisu, I. 1986, ApJS, 61, 479
Harrison, F. A., et al. 1999, ApJ, 523, L121
Hartmann, D., Woosley, S. E., & El Eid, M. F. 1985, ApJ, 297, 837
Hillebrandt, W., Wolff, R. G., & Nomoto, K. 1984, A&A, 133, 175
Hoffman, R. D., Woosley, S. E., & Qian, Y.-Z. 1997, ApJ, 482, 951
Ikhsanov, N. R. 1999, A&A, 347, 915
Ivanova, N., Heinke, C. O., Rasio, F. A., Taam, R. E., Belczynski, K., & Fregeau, J. 2006, MNRAS, 372, 1043
Janka, H. T. 1991, A&A, 244, 378
Karl, C. A., Napiwotzki, R., Heber, U., Dreizler, S., Koester, D., & Reid, I. N. 2005, A&A, 434, 637
Kitaura, F. S., Janka, H.-T., & Hillebrandt, W. 2006, A&A, 450, 345
Koester, D., Dreizler, S., Weidemann, V., & Allard, N. F. 1998, A&A, 338, 612
Kulkarni, S. R., et al. 1999, Nature, 398, 389
Liu, Y. T., & Lindblom, L. 2001, MNRAS, 324, 1063
Livne, E., Burrows, A., Walder, R., Lichtenstadt, I., & Thompson, T. A. 2004, ApJ, 609, 277
Livne, E., Dessart, L., Burrows, A., & Meakin, C. A. 2007, ApJS, 170, 187
Lynden-Bell, D. 1996, MNRAS, 279, 389
——— 2003, MNRAS, 341, 1360
MacFadyen, A. I., & Woosley, S. E. 1999, ApJ, 524, 262
Madau, P., della Valle, M., & Panagia, N. 1998, MNRAS, 297, L17
Mannucci, F., Della Valle, M., Panagia, N., Cappellaro, E., Cresci, G., Maiolino, R., Petrosian, A., & Turatto, M. 2005, A&A, 433, 807
Mayle, R., & Wilson, J. R. 1988, ApJ, 334, 909
Metzger, B. D., Thompson, T. A., & Quataert, E. 2007, 2007, ApJ, 659, 561
Mochkovitch, R., & Livio, M. 1989, A&A, 209, 111
———. 1990, A&A, 236, 378
Nelemans, G., Portegies Zwart, S. F., Verbunt, F., & Yungelson, L. R. 2001a, A&A, 368, 939
Nelemans, G., Yungelson, L. R., Portegies Zwart, S. F., & Verbunt, F. 2001b, A&A, 365, 491
Nomoto, K., Iwamoto, K., Yamaoka, H., & Hashimoto, M. 1995, ASP Conf. Ser. 72: Millisecond Pulsars. A Decade of Surprise, 72, 164
Nomoto, K., & Kondo, Y. 1991, ApJ, 367, L19
Ostriker, J. P., & Bodenheimer, P. 1968, ApJ, 151, 1089
Ott, C. D. 2007, Ph.D. thesis (Univ. Potsdam)
Ott, C. D., Dimmelmeier, H., Marek, A., Janka, H. T., Hawke, I., Zink, B., & Schnetter, E. 2007, Phys. Rev. Lett, 98, 261101
Paczynski, B. 1990, ApJ, 363, 218
Payne, D. J. B., & Melatos, A. 2004, MNRAS, 351, 569
———. 2007, MNRAS, 376, 609
Pessah, M. E., Chan, C.-K., & Psaltis, D. 2006a, Phys. Rev. Lett., 97, 221103
———. 2006b, MNRAS, 372, 183
Pessah, M. E., & Psaltis, D. 2005, ApJ, 628, 879
Qian, Y.-Z., & Woosley, S. E. 1996, ApJ, 471, 331
Rosswog, S. 2007, MNRAS, 376, L48
Ruffert, M., Janka, H.-T., Takahashi, K., & Schaefer, G. 1997, A&A, 319, 122
Scannapieco, E., & Bildsten, L. 2005, ApJ, 629, L85
Segretain, L., Chabrier, G., & Mochkovitch, R. 1997, ApJ, 481, 355
Shakura, N. I., & Sunyaev, R. A. 1973, A&A, 24, 337
Shen, H., Toki, H., Oyamatsu, K., & Sumiyoshi, K. 1998, in Proc. International Conference on Neutron Stars and Pulsars, ed. N. Shibazaki et al. (Tokyo: Universal Academy Press), 157
Shibata, M., Liu, Y. T., Shapiro, S. L., & Stephens, B. C. 2006, Phys. Rev. D, 74, 104026
Taam, R. E., & van de Heuvel, E. P. J. 1986, ApJ, 305, 235
Tan, J. C., Matzner, C. D., & McKee, C. F. 2001, ApJ, 551, 946
Thompson, C., & Duncan, R. C. 1995, ASP Conf. Ser. 72, Millisecond Pulsars: A Decade of Surprise (San Francisco: ASP), 301
Thompson, T. A. 2007, Rev. Mex. AA Conf. Ser., 27, 80
Thompson, T. A., Chang, P., & Quataert, E. 2004, ApJ, 611, 380
Usov, V. V. 1992, Nature, 357, 472
———. 1994, MNRAS, 267, 1035
Uzdensky, D. A., & MacFadyen, A. I. 2006, ApJ, 647, 1192
Valyavin, G., Bagnulo, S., Monin, D., Fabrika, S., Lee, B.-C., Galazutdinov, G., Wade, G. A., & Burlakova, T. 2005, A&A, 439, 1099
van den Heuvel, E. P. J. 2007, in AIP Conf. Proc. 924, The Multicolored Landscape of Compact Objects and Their Explosive Origins (New York: AIP), 598
van den Heuvel, E. P. J., & Bitzaraki, O. 1995, A&A, 297, L41
van Paradijs, J., van den Heuvel, E. P. J., Kouveliotou, C., Fishman, G. J., Finger, M. H., & Lewin, W. H. G. 1997, A&A, 317, L9
Vranevsevic, N., Manchester, R. N., & Melrose, D. B. 2006, in Proc. 63 WE-Heraeus Seminar on Neutron Stars and Pulsars, ed. W. Becker & H. H. Huang (MPE Rep. 291; Garching: MPE), 88
Walder, R., Burrows, A., Ott, C. D., Livne, E., Lichtenstadt, I., & Jarrah, M. 2005, ApJ, 626, 317
Wang, Z., Chakrabarty, D., & Kaplan, D. L. 2006, Nature, 440, 772
Wheeler, J. C., Cowan, J. J., & Hillebrandt, W. 1998, ApJ, 493, L101
Woosley, S. E. 1993, ApJ, 405, 273
Woosley, S. E., & Baron, E. 1992, ApJ, 391, 228
Woosley, S. E., & Hoffman, R. D. 1992, ApJ, 395, 202
Yi, I., & Blackman, E. G. 1997, ApJ, 482, 383
———. 1998, ApJ, 494, L163
Yoon, S.-C., & Langer, N. 2005, A&A, 443, 643
Yoon, S.-C., Langer, N., & Scheithauer, S. 2004, A&A, 425, 217
Yoon, S.-C., Podsiadlowski, P., & Rosswog, S. 2007, MNRAS, submitted (arXiv:0704.0297)
Yungelson, L. R., & Livio, M. 1998, ApJ, 497, 168
———. 2000, ApJ, 528, 108
Zhang, B., & Mészáros, P. 2004, Int. J. Mod. Phys. A, 19, 2385